Enhanced performance in fusion plasmas through turbulence suppression by megaelectronvolt ions

ARTICLES
https://doi.org/10.1038/s41567-022-01626-8
nature physics

Enhanced performance in fusion plasmas through turbulence suppression by megaelectronvolt ions

S. Mazzi[1,2,11]✉, J. Garcia[2]✉, D. Zarzoso[1], Ye. O. Kazakov[3], J. Ongena[3], M. Dreval[4,5], M. Nocente[6,7], Ž. Štancar[8,9], G. Szepesi[9], J. Eriksson[10], A. Sahlberg[10], S. Benkadda[1] and JET Contributors*

Alpha particles with energies on the order of megaelectronvolts will be the main source of plasma heating in future magnetic confinement fusion reactors. Instead of heating fuel ions, most of the energy of alpha particles is transferred to electrons in the plasma. Furthermore, alpha particles can also excite Alfvénic instabilities, which were previously considered to be detrimental to the performance of the fusion device. Here we report improved thermal ion confinement in the presence of megaelectronvolts ions and strong fast ion-driven Alfvénic instabilities in recent experiments on the Joint European Torus. Detailed transport analysis of these experiments reveals turbulence suppression through a complex multi-scale mechanism that generates large-scale zonal flows. This holds promise for more economical operation of fusion reactors with dominant alpha particle heating and ultimately cheaper fusion electricity.

The urgent need for environmentally friendly energy sources is becoming increasingly more important. Among several options, the fusion reaction between the hydrogen isotopes deuterium (D) and tritium (T) holds the promise of safe, clean and almost inexhaustible energy production: $D + T \rightarrow {}^4He\ (3.5\,MeV) + n\ (14.1\,MeV)$, with an alpha particle (^{4}He) and a neutron (n) as fusion products. This reaction needs temperatures of around 150 million kelvin and can be realized in magnetic confinement fusion devices[1]. The largest fusion device currently in operation is the Joint European Torus (JET)[2]. The successor device, the International Thermonuclear Experimental Reactor (ITER), aims to demonstrate the scientific and technological maturity of magnetic confinement fusion[3].

Both JET and ITER are based on the tokamak concept, a toroidal configuration shown schematically in Fig. 1. Large temperature gradients (~100 million kelvin per metre) are unavoidably present in these devices because of the required high plasma temperature in the centre and the necessity for a cold plasma edge. These gradients create instabilities and turbulence, often with very different spatio-temporal scale lengths[4]. One of the most important is the ion temperature gradient (ITG) instability with a characteristic length scale on the order of the ion gyroradius, usually much smaller than the plasma size (for example, ~10^{-3} m versus ~1 m in JET). The microscopic ITG instability largely limits the plasma temperatures that can be achieved in a fusion device[5].

The success of magnetic confinement fusion as an energy source relies crucially on reaching high temperatures for the D and T ions. Fusion-born megaelectronvolt (MeV)-range alpha particles are the main source of central plasma heating in the ITER and future fusion power plants. However, these highly energetic ions primarily heat electrons rather than thermal ions through Coulomb collisions. The extrapolation of plasma heating by alpha particles in future devices is not straightforward, partly because of the effect of fast ions on plasma turbulence. Recent progress in this developing field of research has shown that ion-scale turbulence can be partly reduced in the presence of fast ions with energies of ~100 keV (refs. [6–9]). However, at these energies, fast ions provide dominant bulk ion heating, in strong contrast to the electron heating from alphas in a fusion reactor.

Alpha particles can also excite a range of instabilities that are often considered detrimental to plasma confinement. Modes driven by fast ions can cause increased radial transport of energetic ions[10–13] and enhance plasma turbulence[14]. Among possible instabilities driven by alpha particles in the ITER, toroidicity-induced Alfvén eigenmodes (TAEs)[15,16] are of particular concern[17]. However, numerical analysis[9] has shown that, in plasmas with ion heating from ~100 keV ions, that is, under conditions far from those in a fusion reactor, reduced turbulence can be obtained when TAEs are marginally stable, leaving open the question of whether improved thermal ion confinement can be reached experimentally in plasmas with MeV-range fast ions and fully destabilized TAEs.

Thermal ion energy fluxes perpendicular to the magnetic surfaces can be reduced because of the appearance of intense, poloidally directed shear flows known as zonal flows[18]. In fact, zonal flows, which are solely generated by nonlinear interactions, are a common phenomenon in nature and can be remarkably stable, for example, the famous belts of Jupiter[19]. The generation of zonal flows by energetic ions and fast-ion-driven modes, in particular TAEs, was put forward in simplified contexts in several theoretical studies recently[20,21]. As the dynamics of ITER plasmas will be determined in part by the nonlinear interaction between MeV-range alphas, Alfvén eigenmodes destabilized by these alphas and microturbulence,

[1]Aix-Marseille University, CNRS, PIIM, UMR 7345, Marseille, France. [2]IRFM, CEA, Saint Paul Lez Durance, France. [3]Laboratory for Plasma Physics, LPP-ERM/KMS, TEC Partner, Brussels, Belgium. [4]Institute of Plasma Physics, National Science Center, Kharkiv Institute of Physics and Technology, Kharkiv, Ukraine. [5]V.N. Karazin Kharkiv National University, Kharkiv, Ukraine. [6]University of Milano-Bicocca, Milan, Italy. [7]Institute for Plasma Science and Technology, CNR, Milan, Italy. [8]Slovenian Fusion Association (SFA), Jožef Stefan Institute, Ljubljana, Slovenia. [9]Culham Science Centre, UK Atomic Energy Authority, Abingdon, UK. [10]Department of Physics and Astronomy, Uppsala University, Uppsala, Sweden. [11]Present address: Swiss Plasma Center, École Polytechnique Fédérale de Lausanne (EPFL), Lausanne, Switzerland. *A list of authors and their affiliations appears online. ✉e-mail: samuele.mazzi@epfl.ch; jeronimo.garcia@cea.fr

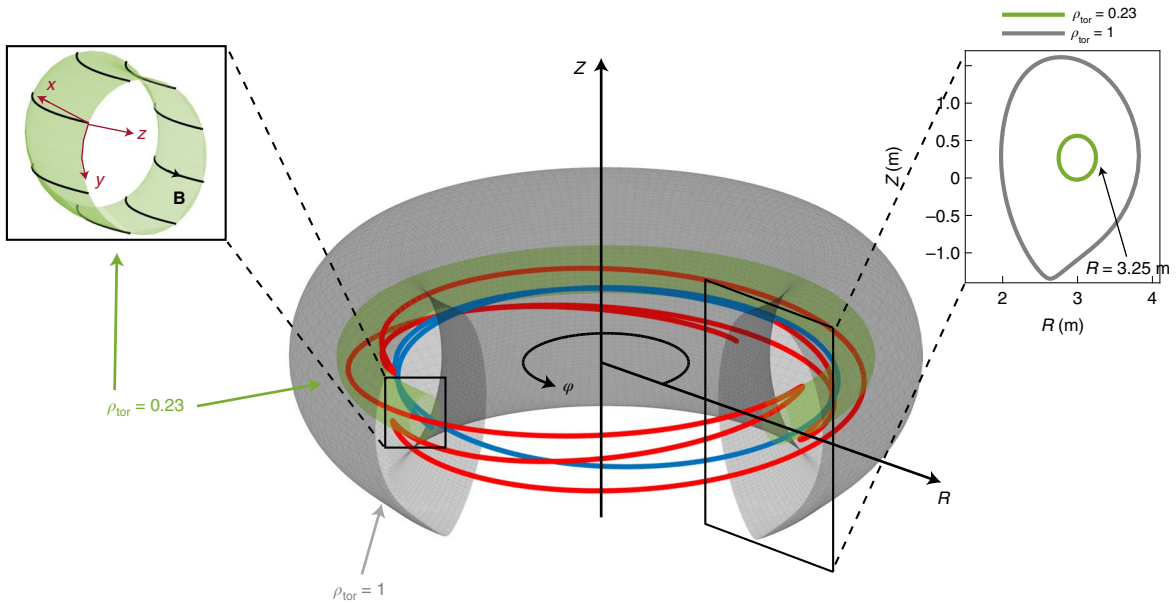

Fig. 1 | Schematic view of the tokamak geometry. Charged particles are confined by a combination of toroidal and poloidal magnetic fields that generate nested surfaces of constant magnetic flux. Passing particles (blue trajectory) circulate along magnetic field lines in the toroidal direction φ, while trapped particles (red trajectory) periodically reverse their parallel velocity with respect to the confining magnetic field **B**. For simplicity, the rapid gyromotion of charged particles is not shown and only the guiding centre motion is displayed. The local transport analysis focuses on the magnetic flux surface corresponding to $\rho_{tor}=0.23$ (green), where ρ_{tor} is the square root of the toroidal magnetic flux normalized to its value at the plasma boundary. The top left inset illustrates the field-aligned set of coordinates used in the flux tube version of the GENE code, with (x, y, z) being the radial, binormal and parallel coordinate, respectively. The top right inset shows a poloidal cross-section of the plasma in the (R, Z) plane for the reported JET experiments, together with the studied flux surface $\rho_{tor}=0.23$ (green) and the plasma boundary $\rho_{tor}=1$ (grey). Here, R is the radial distance from the torus centre and Z is the vertical coordinate. Note that $\rho_{tor}=0.23$ corresponds to $R=3.25$ m at the outboard side.

studying this complex interplay at ITER-relevant conditions becomes an urgent necessity for future progress in fusion science.

In this paper, we identify reproducible conditions and provide experimental evidence for the suppression of ion-scale turbulence in fusion reactor-grade plasmas with strong electron heating from MeV-range fast ions and simultaneously destabilized Alfvén eigenmodes. Corroborated by detailed turbulence analysis, our results pave the way towards enhanced performance of future fusion reactors with strong alpha particle heating.

Improved thermal ion confinement in plasmas with MeV ions

The impact of fast ions on plasma dynamics was studied in JET D–^{3}He plasmas ($n(^3He)/n_e \approx 20$–30%, with n_e the electron density). While the presence of TAEs is usually accompanied by energy loss and particle confinement[10,11,22–24], here we show that reduced ion heat losses and high ion temperatures can be reached in plasmas with MeV-range fast ions and TAEs driven by fast ions. Figure 2 compares JET pulses #94704 (~100 keV ions, blue lines) and #94701 (MeV-range ions, red lines), which were performed at the same operational parameters (L-mode, $B_0=3.7$ T, $I_p=2.5$ MA, $n_{e0}\approx 6\times10^{19}$ m^{-3}, with B_0 the magnetic field, I_p the plasma current and n_{e0} the electron density at the plasma centre) and total auxiliary heating power $P_{aux}=14$MW, but differing in the characteristics of the fast ion population.

In pulse #94704 (Fig. 2, blue lines), Neutral Beam Injection (NBI) was the only heating system, providing fast D ions with energies up to 100 keV. These moderately energetic ions deposit most of their energy to bulk ions, resulting in plasmas with $T_i/T_e>1$ (for example, $T_i/T_e\approx1.4$ measured at $\rho_{tor}=0.2$). The corresponding electron and ion temperature profiles at $P_{aux}=14$ MW (at time $t=9.0$ s) are shown in Fig. 2f,g. The injected fast NBI ions are sub-Alfvénic ($v_{NBI}/v_A\approx0.4$, with v_{NBI} the velocity of the NBI ions and v_A the Alfvén velocity), and no Alfvén eigenmodes were observed in this plasma.

In the comparison pulse #94701 (Fig. 2, red lines), fast D ions from NBI were accelerated to much higher energies (up to ~2–3 MeV; Supplementary Fig. 1) with waves in the ion cyclotron range of frequencies (ICRF) using the three-ion D–(D_{NBI})–^{3}He scheme ($P_{NBI}=8$ MW, $P_{ICRF}=6$ MW)[25–28]. The presence of MeV-range ions resulted simultaneously in long-period sawteeth, destabilization of various Alfvén eigenmodes and the increased plasma stored energy and D–D neutron rate. As a result of the collisional slowing-down, these highly energetic deuterons heat predominantly electrons (similar to alpha particle heating in future fusion reactors), giving rise to a strongly peaked electron temperature profile with much larger T_{e0} (Fig. 2f). Interestingly, the ion temperature in this core electron-heated plasma was at least as high as in the NBI-only pulse #94704 with more ion heating, and $T_i/T_e\approx1$ was reached.

We focus on the transport characteristics in the central region of these plasmas ($\rho_{tor}\lesssim0.4$), where most of the alpha particles will be generated in a future fusion reactor. The electron and thermal ion heat diffusivities computed with TRANSP[29,30] (Fig. 2h,i) show that ions are the primary heat loss channel in the NBI-only pulse #94704 ($\chi_i>\chi_e$). For example, at $\rho_{tor}=0.23$, $\chi_i\approx1.9$ m^2 s^{-1} and $\chi_e\approx0.6$ m^2 s^{-1}. In contrast, in pulse #94701 with highly energetic ions, $\chi_i\approx0.8$ m^2 s^{-1} is much reduced at this radial location, while χ_e remains almost unchanged. Comparison of these two χ_i profiles (Fig. 2i) clearly indicates a significant improvement of the thermal ion confinement in the plasma core of the pulse with electron heating by fast ions. Note that, in the absence of ion temperature measurements at $\rho_{tor}<0.2$, the near-axis χ_i were computed using a global third-order polynomial fit for T_i (as routinely employed in TRANSP modelling of JET experiments), or assuming $T_i=T_e$ (Methods).

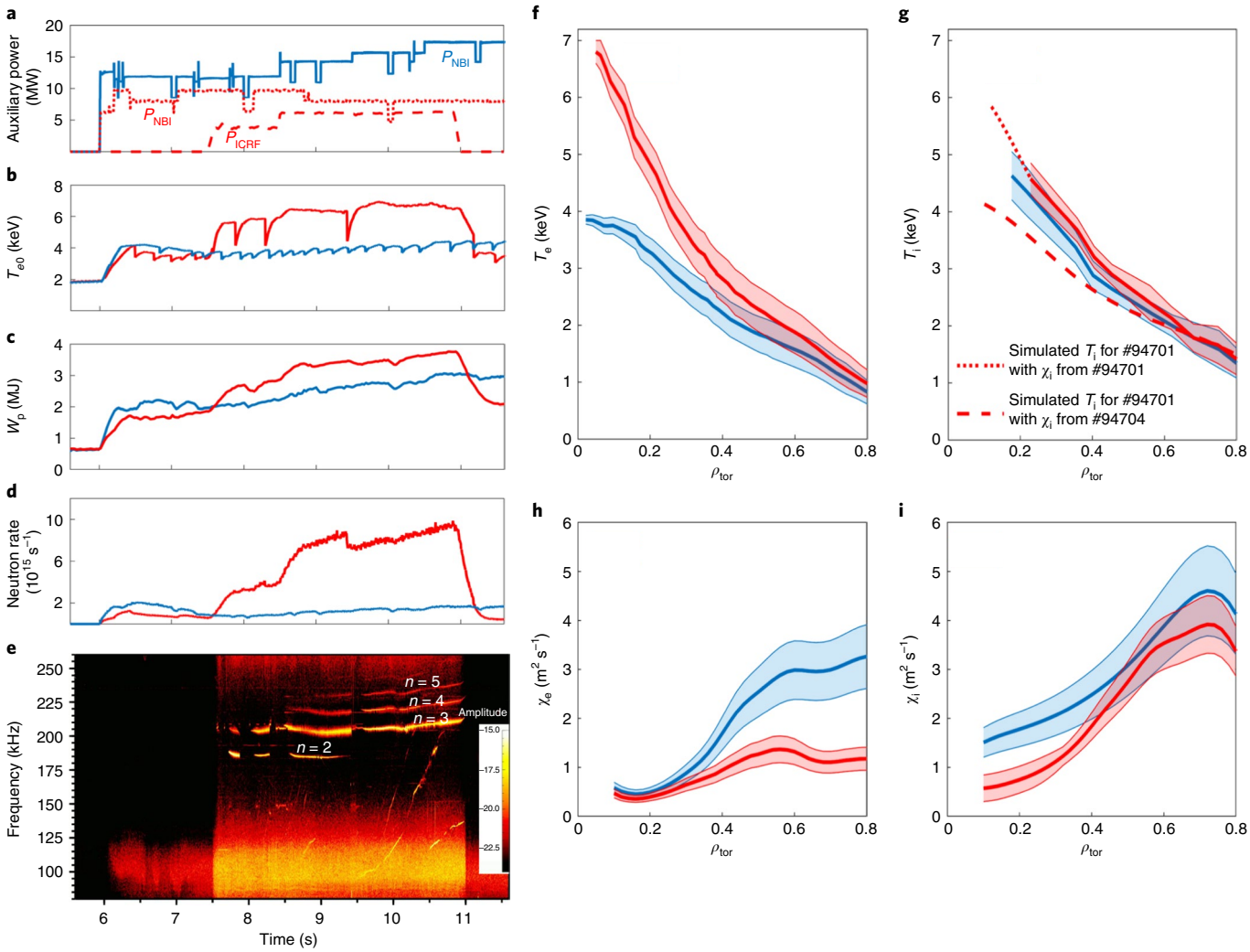

Fig. 2 | Improved thermal ion confinement in fusion plasmas with MeV ions and unstable TAEs. Comparison of two JET pulses #94704 (~100 keV ions, blue lines) and #94701 (MeV-range ions, red lines) performed at the same operational conditions and same total auxiliary heating power $P_{aux}=14$ MW but with different characteristics of the fast ion population. **a**, Auxiliary heating power from the NBI system, P_{NBI}, and the ICRF system, P_{ICRF}. **b**, Core electron temperature, T_{e0}. **c**, Plasma stored energy, W_p. **d**, Neutron rate from D–D fusion reactions. **e**, Magnetic coil spectrogram showing destabilized TAEs with different toroidal mode numbers, n, in pulse #94701. **f**,**g**, Measured radial profiles of the electron (T_e, **f**), and ion temperatures (T_i, **g**) at $P_{aux}=14$ MW, where ρ_{tor} is the square root of the toroidal magnetic flux normalized to its value at the plasma boundary. The error bands in both panels account for the standard deviation of the time-averaged (±0.1 s) signals and the systematic diagnostic uncertainties. **h**,**i**, Computed electron (χ_e, **h**) and thermal ion (χ_i, **i**) heat diffusivities as a function of ρ_{tor}. The error bands in these panels take into account uncertainties in the temperature profile data, different fittings to T_i and the extrapolation to the magnetic axis, including uncertainties in the power balance. Dotted and dashed red lines in **g** show the T_i profiles for pulse #94701 predicted using the two χ_i profiles in **i** as input.

As a next step, predictive modelling of T_i in pulse #94701 was undertaken with the CRONOS code[31], using all relevant parameters, including measured T_e and n_e, and heat source profiles calculated by TRANSP as input. Two different χ_i profiles were assumed in this analysis (Fig. 2i). The impact of the reduced ion heat losses on the T_i achieved in #94701 is clearly illustrated by comparing the two predicted T_i profiles shown in Fig. 2g. The dotted red line illustrates the ion temperature in #94701 predicted using the TRANSP-computed χ_i for this pulse. The good agreement between the predicted and measured T_i profiles verifies the consistency of CRONOS and this synthetic modelling approach. This analysis also shows that a much lower T_i would have been reached in #94701 (dashed red line) if the thermal ion heat diffusivity were the same as in the NBI-only pulse #94704. However, the experimentally observed T_i in #94701 is significantly larger than the latter T_i prediction, providing further confirmation of the reduced ion heat losses in the presence of MeV ions.

The well-known mechanisms stabilizing ITG turbulence such as the ratio T_i/T_e and the $\mathbf{E}\times\mathbf{B}$ shearing rate ($\gamma_{E\times B}$) cannot explain the lower χ_i in the core region ($\rho_{tor}<0.4$) for pulse #94701. Indeed, both parameters are lower in this pulse as compared with those in the NBI-only pulse #94704. For example, at $\rho_{tor}=0.23$, $T_i/T_e\approx1$ versus 1.4 and $\gamma_{E\times B}\approx1.4\,\mathrm{m\,s^{-1}}$ versus $2.2\,\mathrm{m\,s^{-1}}$.

The two comparison pulses are not only inherently different in the heating channel for fast ions (dominant ion versus electron heating) but also feature an essential difference in the magnetohydrodynamic (MHD) behaviour. The sub-Alfvénic NBI ions in #94704 did not destabilize any Alfvén eigenmodes. In contrast, a variety of TAE modes in the frequency range ~200 kHz with toroidal mode numbers $n=2$–6 were driven by high-energy ions in pulse #94701 (Fig. 2e). The observed mode frequencies are in good agreement with the theoretically predicted frequencies of TAEs, $f_{TAE}^{(lab)}=f_{TAE}^{(plasma)}+nf_{rot}$. In this formula,

Table 1 | Plasma parameters used in the GENE modelling of JET pulse #94701 at $\rho_{tor} = 0.23$ and $t \approx 9.6$ s

R_0 (m)	B_0 (T)	ϵ	q	$\hat{s}$	n_e (m^{-3})	n_D/n_e	$n_{^3He}/n_e$	n_{FD}/n_e
3.0	3.7	0.31	1.1	0.63	5.2×10^{19}	0.43	0.27	0.03
R/L_{n_e}	R/L_{n_D}	$R/L_{n_{^3He}}$	T_e (keV)	T_i/T_e	T_{FD}/T_e	$R/L_{T_{e,i}}$	β_e (%)	ν^*
4.5	3.7	5.0	4.4	1.0	33.8	10.3	0.68	9.4×10^{-5}

Here, R_0 is the major radius, B_0 is the on-axis magnetic field, ϵ is the inverse aspect ratio, q and $\hat{s}$ are the local safety factor and magnetic shear, respectively, n_j and T_j are the local density and temperature of various plasma species (electrons, thermal D and ^{3}He ions, and fast D ions), $R/L_{n,T}$ is the normalized logarithmic density and temperature gradient, β_e is the electron beta and ν^* is the normalized collision frequency. The reported input parameters are common to all the numerical GENE simulation cases. The various cases, however, differ essentially in the normalized logarithmic fast ion pressure gradient $R/L_{p_{FD}}$, whose values are displayed in Fig. 3.

$f_{TAE}^{(plasma)} = v_{A0}/(4\pi q_{TAE} R_0) \approx 166 - 191$ kHz, $q_{TAE} \simeq 1 + 1/(2n) \approx 1.1-1.3$ (ref. [24]) is the value of the safety factor at the TAE location, v_{A0} is the Alfvén velocity in the plasma centre and $f_{rot} \approx 7-8$ kHz is the local plasma rotation frequency, as measured by the Charge eXchange Recombination Spectroscopy system. The localization of TAEs outside the $q=1$ surface in this ICRF + NBI plasmas has been confirmed independently by correlation reflectometer measurements, indicating that the radial range of the TAEs is $R_{TAE} \approx 3.22-3.36$ m (Supplementary Fig. 3a).

The correlation reflectometer also provides local density fluctuation spectra, which can be used to characterize the turbulence characteristics in the plasma. Such analysis performed at $R = 3.25$ m and $R = 3.3$ m (Supplementary Fig. 3b,c) highlights that the lowest fluctuation amplitudes were reached in plasmas with MeV-range fast ions and destabilized TAEs. Furthermore, a clear reduction of the thermal ion heat diffusivity was observed at these radial locations (Fig. 2i). As the characteristics of the fast ions in pulse #94701 ($T_{fast}/T_e \approx 34$ and $n_{fast}/n_e \approx 3\%$, with T_{fast} and n_{fast} the temperature and density of the fast D ions) are close to the predicted conditions for alpha particles in ITER[32], the identified mechanism holds promise for optimizing the performance of future fusion reactors with strong alpha particle heating.

Note that the sawtooth dynamics observed in pulse #94701 is similar to findings in earlier JET experiments with ICRF and monster sawteeth[33,34]. However, in strong contrast to ref. [33], a much smaller plasma volume was enclosed within the sawtooth inversion radius in the JET experiments reported herein, thereby limiting the impact of the sawtooth stabilization itself on the improved plasma confinement. Note also that the power balance analysis used in this paper to infer the thermal conductivities ignores any possible anomalous ion heating effects such as, for example, reported in ref. [35]. In the absence of reliable measurements of high-frequency Alfvén eigenmodes (>1 MHz), their potential impact in the reported plasmas is difficult to assess.

Numerical modelling of turbulence suppression

These JET experimental observations are corroborated by modelling with the local (or 'flux-tube') version of the state-of-the-art gyrokinetic code GENE[36] that successfully reproduced turbulence properties for various tokamak experiments (see, for example, refs. [6,7,37–39]). For analysis of JET pulse #94701, we choose a flux tube around $\rho_{tor} = 0.23$ ($R = 3.25$ m) as this region is characterized by large temperature gradients and a significant population of fast ions and TAEs. Table 1 summarizes the modelling input data. An equivalent Maxwellian distribution was used to represent the population of fast deuterons. Linear stability analysis shows that, as expected, ITG modes dominate the spectrum, peaking at $k_y\rho_s \approx 0.45$, where k_y is the binormal ('poloidal') wavenumber and ρ_s is the characteristic Larmor radius of thermal ions at the reference sound speed, defined in this paper as $c_s = (T_e/m_p)^{1/2}$, where m_p is the proton mass.

Because of the uncertainties in the fast ion profiles calculated by TRANSP in the presence of destabilized Alfvén eigenmodes and the limitations of the Maxwellian approximation to represent fully the detailed fast ion distribution, a scan over the normalized logarithmic fast ion pressure gradient, $R/L_{p_{FD}}$ (with $L_{p_{FD}}$ the inverse logarithmic pressure gradient), was performed. This allows to compensate the discrepancy induced by the derivative in velocity space by fine-tuning the radial gradient of the fast ion temperature and density profiles. Furthermore, as part of this assessment, we find that, for $R/L_{p_{FD}} > 10.7$, fast D ions destabilize ballooned modes with frequencies $f \approx 200$ kHz and $k_y\rho_s$ between 0.025 and 0.05, corresponding to $n = 4-7$. As all of these mode characteristics match well with those of the experimentally measured TAEs (Fig. 2e), these high-frequency modes appearing in the GENE simulations are identified as fast-ion-driven TAEs.

This analysis was followed by nonlinear GENE simulations. Figure 3a shows the heat diffusivity attributed to electrostatic fluctuations for both thermal ion species, χ_{ES}(D) and χ_{ES}(^{3}He). Figure 3b–d illustrates the amplitudes of the Fourier components normalized to their maximum, $\hat{\phi}_n$, of the perturbed electrostatic potential ϕ (averaged over the radial and parallel directions) as a function of frequency and $k_y\rho_s$. The frequency dependence of $\hat{\phi}_n$, additionally averaged over $k_y\rho_s$, is illustrated in Fig. 3e–g. The turbulence spectra reveal that, for $R/L_{p_{FD}} \approx 6$, the dominant modes are characterized by low frequencies and peak at around $k_y\rho_s \approx 0.2$. These k_y values are somewhat lower than in linear simulations. This is typical for local gyrokinetic modelling and is linked to the inverse cascade of energy, in which modes with larger k_y transfer energy to modes with lower k_y. At larger fast ion gradients, for example, at $R/L_{p_{FD}} \approx 16$, the turbulence structure is modified substantially. The dominant modes are shifted towards higher frequencies $f \approx 200$ kHz and lower $k_y\rho_s \approx 0.025-0.05$, matching closely the characteristics of the observed TAEs.

Figure 3a clearly shows a strong stabilizing effect of fast ions on ion-scale turbulence when fast-ion-driven TAEs appear in nonlinear GENE simulations. See, for example, Fig. 3g computed for $R/L_{p_{FD}} \approx 16$. Under these conditions, the computed electrostatic diffusivities χ_{ES} of both thermal ion species are reduced by more than 95% compared with the values obtained without fast ions, and agree well with χ_i computed by TRANSP (Fig. 3a, dashed black line). However, the predicted GENE value $\chi_e \approx 3.5\,m^2\,s^{-1}$ is significantly larger than the electron heat diffusivity obtained from TRANSP ($\chi_e \approx 0.5\,m^2\,s^{-1}$). To obtain better agreement between the GENE and power balance results, an additional set of nonlinear simulations was performed but varying the input parameters within experimental uncertainties. Consistency in both χ_i and χ_e was achieved simultaneously at $R/L_{p_{FD}} \approx 14$ with temperature gradients reduced by 15% (Fig. 3c,f), yielding $\chi_e \approx 0.7\,m^2\,s^{-1}$. This result supports the observation of high T_{e0} in JET pulse #94701, in contrast to earlier results from the National Spherical Torus Experiment (NSTX) where the electron confinement was strongly degraded in the presence of Alfvén eigenmodes[40].

Note that modes at $f \approx 20-30$ kHz were observed in pulse #94701. Modes at similar frequencies also appeared in the GENE simulations at $R/L_{p_{FD}} \approx 14$ and 16. The bispectral analysis of the electrostatic potential indicates a nonlinear coupling between these

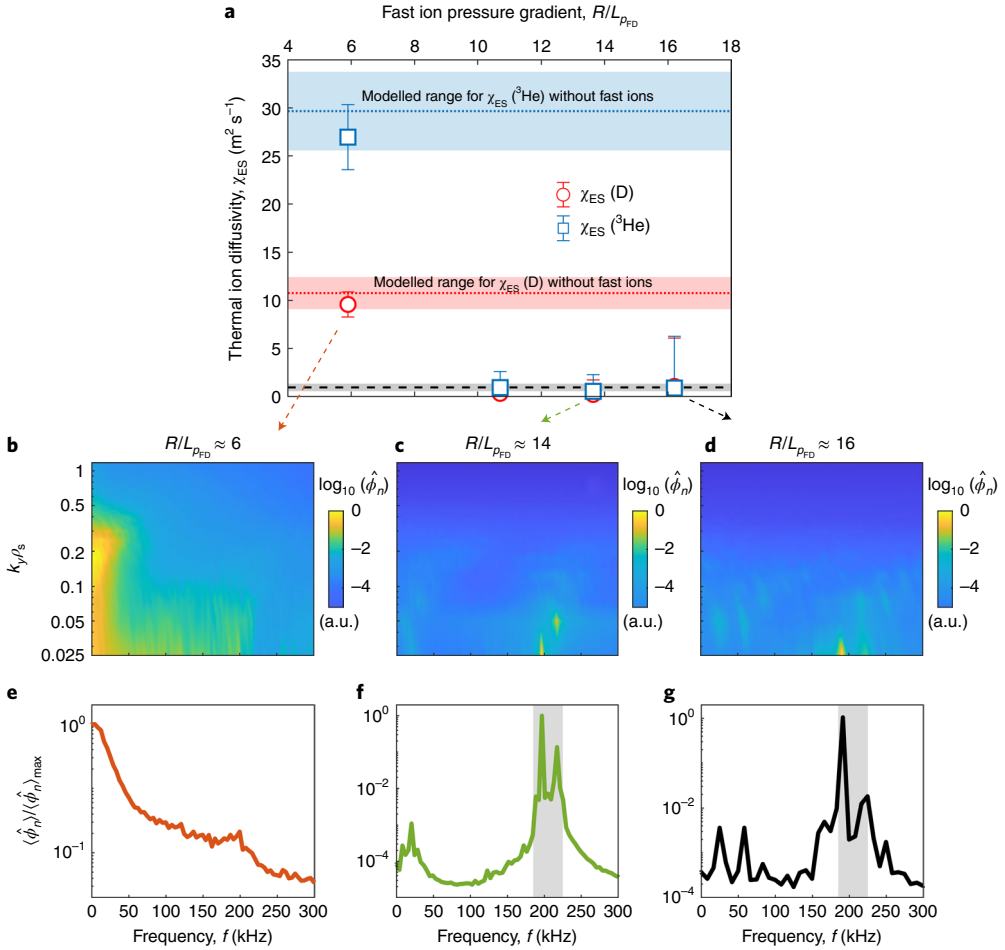

Fig. 3 | Thermal ion transport suppression in plasmas with MeV ions and fast-ion-driven modes. a, Electrostatic thermal diffusivities χ_{ES} as simulated by GENE for D and ^{3}He ions against the normalized logarithmic fast ion pressure gradient $R/L_{p_{FD}}$ as predicted by GENE. **b**–**d**, Contour plots of the Fourier components normalized to their maximum, $\hat{\phi}_n$ of the perturbed electrostatic potential ϕ (averaged over the radial and parallel directions) as a function of frequency and $k_y\rho_s$, where k_y is the binormal wavenumber and ρ_s is the characteristic ion Larmor radius, for $R/L_{p_{FD}}$ of 6 (**b**), 14 (**c**) and 16 (**d**). **e**–**g**, Frequency dependence of $\hat{\phi}_n$, additionally averaged over $k_y\rho_s$ (indicated by the symbol $\langle\ldots\rangle$), for $R/L_{p_{FD}}$ of 6 (**e**), 14 (**f**) and 16 (**g**). In **f** and **g**, grey areas indicate the experimentally measured TAE frequency range. In **a**, the error bars of GENE time-dependent simulations represent the standard deviation obtained from the code calculation. The large error bars for the rightmost points can be attributed to the high-frequency and large-amplitude modulations of the energy fluxes due to strong fast-ion-driven fluctuations of the electrostatic potential. Horizontal dotted lines and associated shaded areas in **a** represent thermal ion diffusivities and their standard deviations for the GENE modelling case without fast ions. The dashed line at the bottom of **a** shows the computed thermal ion heat diffusivity for JET pulse #94701 ($\chi_i = 0.8\,m^2\,s^{-1}$) as given by TRANSP, while the grey-shaded area corresponds to the error band in Fig. 2i.

modes and TAEs, similar to results reported in ref. [41]. However, since turbulence suppression is reached in GENE simulations already at $R/L_{p_{FD}} \approx 11$, when such a mode coupling is not observed, we exclude these low-frequency modes as a main cause for the observed confinement improvement.

Figure 4a–c illustrates the dependence of the perturbed electrostatic potential ϕ on the radial (x/ρ_s) and binormal (y/ρ_s) coordinates. In the absence of fast ions (Fig. 4a), small-scale turbulent eddies predominately elongated along the radial direction, typical for ITG-induced transport, are seen. In contrast, Fig. 4b,c shows the sudden appearance of intense, poloidally oriented and radially sheared zonal flows in GENE simulations at $R/L_{p_{FD}} \approx 14$ and $R/L_{p_{FD}} \approx 16$, corresponding to plasmas with MeV ions and destabilized TAEs. In these cases, the zonal flow shearing rate reaches $\gamma_{E\times B,zonal} \approx 0.84c_s/a$ and $0.86c_s/a$, respectively, almost twice the value without fast ions ($0.48c_s/a$), with a the minor radius. These zonal flows strongly affect the ITG nonlinear saturation[18] and produce a radial de-correlation of the turbulent eddies[42], thereby leading to a reduction in the turbulent transport. Furthermore, Fig. 4e,f illustrates the appearance of zonal structures also in the perturbed magnetic potential with unstable TAEs, consistent with earlier analytical studies[21]. The strong coupling between fast-ion-driven modes and zonal components, previously shown in simplified contexts[20,21], is further highlighted by the bispectral analysis. This analysis suggests a net energy transfer from TAEs to the zonal modes (Supplementary Fig. 6).

The robustness of the GENE results was further checked against the uncertainty in the input R/L_{T_i}, arising from a lack of T_i data at $\rho_{tor} < 0.2$ (see also Methods). The mechanism is reproducible and robust against unavoidable assumptions and simplifications of the local approach.

Experimental evidence for minimized density fluctuations

These modelling predictions of turbulence suppression are supported by the observation of a reduced amplitude of the density fluctuations in these JET plasmas, in particular in pulse #95669, which was performed at very similar plasma conditions to #94701. Supplementary Fig. 3b,c shows that much smaller density fluctuation

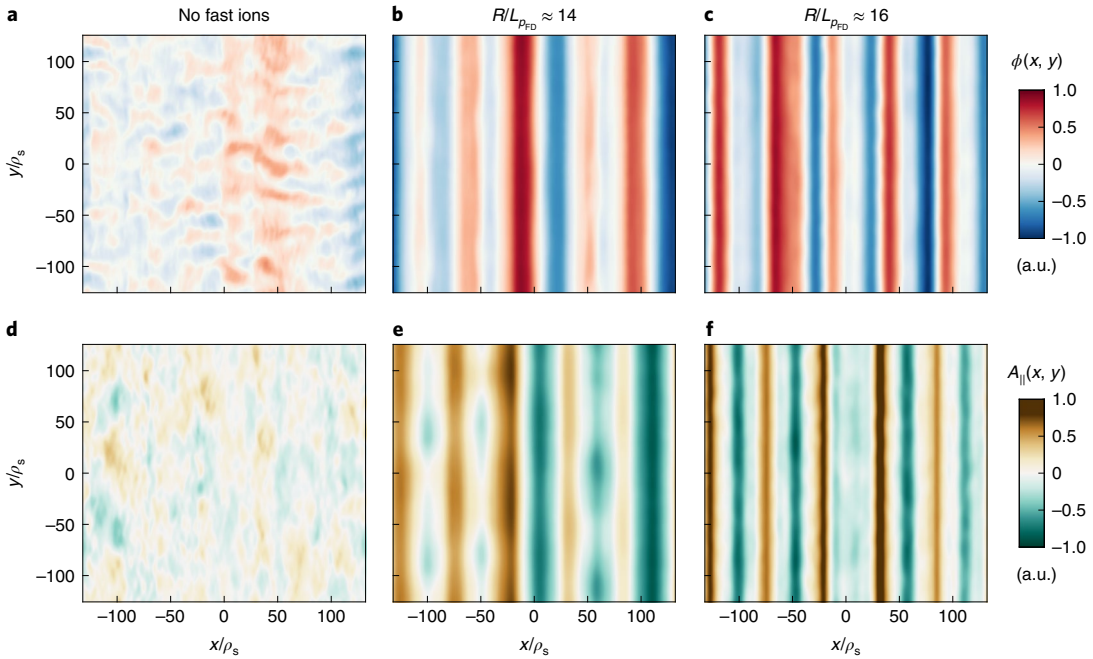

Fig. 4 | Evidence for the nonlinear generation of zonal structures. a–f, Contour plots of the gyroaveraged perturbed electrostatic potential (ϕ, **a**–**c**) and the component of the vector potential parallel to the magnetic field ($A_{||}$, **d**–**f**) for different fast ion pressure gradients $R/L_{p_{FD}}$ along the radial x and binormal y coordinates, normalized to the characteristic ion Larmor radius ρ_s for modelling without fast ions (**a**,**d**), and for the fast ion case with $R/L_{p_{FD}} \approx 14$ (**b**,**e**) and $R/L_{p_{FD}} \approx 16$ (**c**,**f**). All contour plots are normalized to the corresponding maximum value. This figure clearly shows the appearance of zonal structures leading to turbulence suppression in plasmas with MeV-range ions and fast-ion-driven TAEs.

amplitudes were observed in the plasma phase with MeV-range fast ions and fast-ion-driven TAEs, as compared with the NBI-only phase. As outlined above, partial turbulence reduction in the presence of moderately energetic ions (of a few hundred keV) does not necessarily require TAEs and has been extensively reported[6–9]. This has also been observed in this series of JET experiments, for example, in pulse #95672 (Supplementary Fig. 3), where the application of the three-ion scheme with $P_{ICRF} = 2.1$ MW resulted in monster sawteeth, while TAEs were not destabilized. However, a much stronger reduction was measured in the same JET pulse when the ICRF power was increased to 6 MW such that MeV-range ions and fast-ion-driven TAEs were present in the plasma. Supplementary Fig. 4c clearly illustrates the efficacy of the turbulence suppression mechanism discovered in these JET experiments.

A promising result for ITER and future fusion devices

These promising JET results indicate that unexpected favourable conditions might be realized in ITER and future fusion power plants, where alpha particles provide a strong source of core electron heating[43]. As fast alphas can simultaneously destabilize TAEs at large plasma volumes in ITER[17], this complex mechanism (if present) would provide a significant increase in plasma confinement. However, TAEs can also enhance the fast particle transport, so the final result would depend on a delicate balance between different, competing effects. Predicting the actual TAE mode stability and the efficiency of turbulence suppression in ITER plasmas is challenging because of the sensitivity to radial profiles of background quantities or the energetic particle distributions. Therefore, whether this favourable mechanism of turbulence stabilization will actually materialize in ITER plasmas is an open question. However, the results shown in this paper pave the way to an enhanced realization of fusion as an energy source, which is worth exploring further both experimentally and theoretically in the future.

Online content

Any methods, additional references, Nature Research reporting summaries, source data, extended data, supplementary information, acknowledgements, peer review information; details of author contributions and competing interests; and statements of data and code availability are available at https://doi.org/10.1038/s41567-022-01626-8.

Received: 30 October 2020; Accepted: 4 May 2022;
Published online: 30 June 2022

References

1. Ongena, J., Koch, R., Wolf, R. & Zohm, H. Magnetic-confinement fusion. *Nat. Phys.* **12**, 398–410 (2016).
2. Litaudon, X. et al. Overview of the JET results in support to ITER. *Nucl. Fusion* **57**, 102001 (2017).
3. Shimada, M. et al. Chapter 1: overview and summary. *Nucl. Fusion* **47**, S1–S17 (2007).
4. Doyle, E. J. et al. Chapter 2: plasma confinement and transport. *Nucl. Fusion* **47**, S18–S127 (2007).
5. Romanelli, F. Ion temperature-gradient-driven modes and anomalous ion transport in tokamaks. *Phys. Fluids B* **1**, 1018–1025 (1989).
6. Citrin, J. et al. Nonlinear stabilization of tokamak microturbulence by fast ions. *Phys. Rev. Lett.* **111**, 155001 (2013).
7. Garcia, J. et al. Key impact of finite-beta and fast ions in core and edge tokamak regions for the transition to advanced scenarios. *Nucl. Fusion* **55**, 053007 (2015).
8. Di Siena, A., Görler, T., Doerk, H., Poli, E. & Bilato, R. Fast-ion stabilization of tokamak plasma turbulence. *Nucl. Fusion* **58**, 054002 (2018).
9. Di Siena, A. et al. Electromagnetic turbulence suppression by energetic particle driven modes. *Nucl. Fusion* **59**, 124001 (2019).
10. Fasoli, A. et al. Chapter 5: physics of energetic ions. *Nucl. Fusion* **47**, S264–S284 (2007).
11. Gorelenkov, N., Pinches, S. D. & Toi, K. Energetic particle physics in fusion research in preparation for burning plasma experiments. *Nucl. Fusion* **54**, 125001 (2014).
12. Todo, Y. Introduction to the interaction between energetic particles and Alfvén eigenmodes in toroidal plasmas. *Rev. Mod. Plasma Phys.* **3**, 1 (2019).

13. Heidbrink, W. W. & White, R. B. Mechanisms of energetic-particle transport in magnetically confined plasmas. *Phys. Plasmas* **27**, 030901 (2020).
14. Zarzoso, D. et al. Impact of energetic-particle-driven geodesic acoustic modes on turbulence. *Phys. Rev. Lett.* **110**, 125002 (2013).
15. Cheng, C. Z. & Chance, M. S. Low-*n* shear Alfvén spectra in axisymmetric toroidal plasmas. *Phys. Fluids* **29**, 3695–3701 (1986).
16. Fu, G. Y. & Van Dam, J. W. Excitation of the toroidicity-induced shear Alfvén eigenmode by fusion alpha particles in an ignited tokamak. *Phys. Fluids B* **1**, 1949–1952 (1989).
17. Pinches, S. D. et al. Energetic ions in ITER plasmas. *Phys. Plasmas* **22**, 021807 (2015).
18. Diamond, P. H., Itoh, S. I., Itoh, K. & Hahm, T. S. Zonal flows in plasmas – a review. *Plasma Phys. Control. Fusion* **47**, R35–R161 (2005).
19. Heimpel, M., Aurnou, J. & Wicht, J. Simulation of equatorial and high-latitude jets on Jupiter in a deep convection model. *Nature* **438**, 193–196 (2005).
20. Todo, Y., Berk, H. L. & Breizman, B. N. Nonlinear magnetohydrodynamic effects on Alfvén eigenmode evolution and zonal flow generation. *Nucl. Fusion* **50**, 084016 (2010).
21. Qiu, Z., Chen, L. & Zonca, F. Effects of energetic particles on zonal flow generation by toroidal Alfvén eigenmode. *Phys. Plasmas* **23**, 090702 (2016).
22. Chen, L. & Zonca, F. Physics of Alfvén waves and energetic particles in burning plasmas. *Rev. Mod. Phys.* **88**, 015008 (2016).
23. Breizman, B. N. & Sharapov, S. E. Major minority: energetic particles in fusion plasmas. *Plasma Phys. Control. Fusion* **53**, 054001 (2011).
24. Heidbrink, W. W. Basic physics of Alfvén instabilities driven by energetic particles in toroidally confined plasmas. *Phys. Plasmas* **15**, 055501 (2008).
25. Kazakov, Y. O. et al. Efficient generation of energetic ions in multi-ion plasmas by radio-frequency heating. *Nat. Phys.* **13**, 973–978 (2017).
26. Ongena, J. et al. Synergetic heating of D-NBI ions in the vicinity of the mode conversion layer in H–D plasmas in JET with the ITER like wall. *EPJ Web Conf.* **157**, 02006 (2017).
27. Nocente, M. et al. GENEration and observation of fast deuterium ions and fusion-born alpha particles in JET D–^{3}He plasmas with the 3-ion radio-frequency heating scenario. *Nucl. Fusion* **60**, 124006 (2020).
28. Kazakov, Y. O. et al. Physics and applications of three-ion ICRF scenarios for fusion research. *Phys. Plasmas* **28**, 020501 (2021).
29. Hawryluk, R. J. in *Physics of Plasmas Close to Thermonuclear Conditions* Vol. 1 (eds Coppi B. et al.) 19–46 (Pergamon Press, 1981).
30. Ongena, J., Voitsekhovitch, I., Evrard, M. & McCune, D. Numerical transport codes. *Fusion Sci. Technol.* **61**, 180–189 (2012).
31. Artaud, J. F. et al. The CRONOS suite of codes for integrated tokamak modelling. *Nucl. Fusion* **50**, 043001 (2010).
32. Garcia, J., Görler, T. & Jenko, F. Isotope and fast ions turbulence suppression effects: consequences for high-β ITER plasmas. *Phys. Plasmas* **25**, 055902 (2018).
33. Campbell, D. J. et al. Stabilization of sawteeth with additional heating in the JET tokamak. *Phys. Rev. Lett.* **60**, 2148–2151 (1988).
34. Graves, J. P. et al. Experimental verification of sawtooth control by energetic particles in ion cyclotron resonance heated JET tokamak plasmas. *Nucl. Fusion* **50**, 052002 (2010).
35. Gates, D. A., Gorelenkov, N. N. & White, R. B. Ion heating by fast-particle-induced Alfvén turbulence. *Phys. Rev. Lett.* **87**, 205003 (2001).
36. Jenko, F., Dorland, W., Kotschenreuther, M. & Rogers, B. N. Electron temperature gradient driven turbulence. *Phys. Plasmas* **7**, 1904–1910 (2000).
37. Citrin, J. et al. Electromagnetic stabilization of tokamak microturbulence in a high-β regime. *Plasma Phys. Control. Fusion* **57**, 014032 (2014).
38. Görler, T. et al. On the validation of gyrokinetic L-mode simulations. *Fusion Sci. Technol.* **69**, 537–545 (2016).
39. Mazzi, S. et al. Impact of fast ions on a trapped-electron-mode dominated plasma in a JT-60U hybrid scenario. *Nucl. Fusion* **60**, 046026 (2020).
40. Gorelenkov, N. N. et al. Anomalous electron transport due to multiple high frequency beam ion driven Alfvén eigenmodes. *Nucl. Fusion* **50**, 084012 (2010).
41. Crocker, N. A. et al. Three-wave interactions between fast-ion modes in the national spherical torus experiment. *Phys. Rev. Lett.* **97**, 045002 (2006).
42. Biglari, H., Diamond, P. H. & Terry, P. W. Influence of sheared poloidal rotation on edge turbulence. *Phys. Fluids B* **2**, 1–4 (1990).
43. Stix, T. H. Heating of toroidal plasmas by neutral injection. *Plasma Phys.* **14**, 367–384 (1972).

Methods

GENE simulation model and input parameters. In its flux-tube version, the GENE code solves the nonlinear gyrokinetic Vlasov equations[44] coupled to Maxwell's equations on a field-aligned set of spatial coordinates (see the top left inset of Fig. 1 for a schematic representation). This system of coordinates allows the exploitation of the strong anisotropy of the turbulent fluctuations in directions parallel and perpendicular to the background magnetic field. Whereas the parallel spatial direction z employs a finite-difference solution technique, the perpendicular direction is treated with spectral methods, and hence the radial x and binormal y coordinates in the Fourier domain are generally referred to as k_x and k_y, respectively. The two velocity dimensions employed in GENE are the parallel velocity $v_{\parallel}$ and the magnetic moment μ. A detailed description and derivation of the model equations employed in the flux-tube version can be found in refs. [36,45].

In the present work, both the perpendicular and parallel magnetic field fluctuations are computed, and the collisions are retained. In GENE, Maxwellian distribution functions are employed for all the particle populations, including fast D ions. For the fast ion distribution, the effective density and temperature were calculated from the TRANSP distribution. The number of grid points used in the nonlinear simulations is ($n_{k_x} = 256$, $n_{k_y} = 48$, $n_z = 32$, $n_{v_{||}} = 48$, $n_\mu = 64$) for four different particle populations, that is, electrons, thermal D and ^{3}He ions, and fast D ions. The minimum wavenumber in the binormal direction considered is $k_{y,\min}\rho_s = 0.025$. The employed numerical discretization was chosen after extensive convergence tests, even in the nonlinear phase. Note that, in the simulations without fast particles, the velocity space is relaxed to a less demanding numerical grid. Namely, the number of points in the μ direction is set to $n_\mu = 16$. Indeed, to accurately resolve the high-frequency resonances in fast ion velocity space, the non-equidistant Gauss–Legendre discretization in this direction has to be increased to $n_\mu = 64$. Also, for a more comprehensive description of the numerical implementation techniques and adopted schemes employed in GENE, one can consult dedicated PhD theses, for example, ref. [45], which are available on the GENE website. The input parameters that have been employed in the numerical analyses are reported in Table 1.

The energy flux observable is used to evaluate the radial energy transport computed by the GENE code and compare it with the experimental power balances. The definition of the flux-surface averaged energy flux in the radial direction is

$$\langle Q_j \rangle = \langle \int \mathrm{d}^3 v \frac{1}{2} m_j v^2 f_j(\mathbf{x}, \mathbf{v}) \mathbf{v}_{\mathbf{E}\times\mathbf{B}}(\mathbf{x}) \rangle,$$

where $\mathbf{x} = (x, y, z)$ and $\mathbf{v} = (v_{\parallel}, \mu)$, $\langle \cdot \rangle$ denotes the flux-surface average, $f_j(\mathbf{x}, \mathbf{v})$ is the distribution function, $\mathbf{v}_{\mathbf{E}\times\mathbf{B}} = \frac{c}{B_0^2}\mathbf{B}_0 \times \nabla\bar{\xi}$ is the generalized $\mathbf{E}\times\mathbf{B}$ drift velocity, with $\bar{\xi} = \bar{\phi} - \frac{v_{\parallel}}{c}\bar{A}_{\parallel} + \frac{\mu}{q_j}\bar{B}_{\parallel}$ the gyro-averaged modified potential (in which q_j is the charge and the overbar indicates a gyro-averaged quantity), and the subscript j refers to the species. From this definition, it is possible to appreciate the contributions to the energy flux of the electrostatic potential $\bar{\phi}$, the vector potential $\bar{A}_{\parallel}$ and the parallel magnetic fluctuation $\bar{B}_{\parallel}$ due to the $\mathbf{v}_{\mathbf{E}\times\mathbf{B}}$ drift. Therefore, the electrostatic contribution, which includes only the terms with $\bar{\phi}$, and the electromagnetic contribution, which includes the terms with $\bar{A}_{\parallel}$ and $\bar{B}_{\parallel}$ can be separated. In addition, it is also possible to determine the flux-surface averaged thermal diffusivities $\langle \chi_j \rangle$ from the energy flux as

$$\langle \chi_j \rangle = \frac{\langle Q_j \rangle}{n_{0,j} T_{0,j} \omega_{T,j}}$$

where $\omega_{T,j} = -\frac{a}{T_{0,j}}\frac{\mathrm{d}T_j}{\mathrm{d}x}$ is the normalized temperature gradient of the considered species j. For a more detailed derivation in GENE units of the energy flux and diffusivity, consult, for example, ref. [46].

Interpretive integrated modelling framework. Both pulses #94701 and #94704 were analysed through interpretive simulations performed with the TRANSP modelling suite[30] coupled with the external heating modules NUBEAM (NBI)[47] and TORIC (ICRF)[48], and prepared with the OMFIT integrated modelling platform[49]. The interpretive analysis was based on the use of fitted profiles, including electron density and temperature. The fitting procedures for both quantities were based on high-resolution Thomson scattering measurements, while the temperature was additionally constrained by electron cyclotron emission data, up to the availability of the experimental measurements. To extrapolate the ion temperature profiles to the magnetic axis, two different approaches were used for pulse #94701: (1) assuming $T_i = T_e$ in the region $\rho_{\mathrm{tor}} \lesssim 0.2$ in combination with the available high-resolution T_e data or (2) applying a global third-order polynomial fit in the range $\rho_{\mathrm{tor}} \lesssim 0.8$ (with the additional constraint $\partial T_i(0)/\partial r = 0$). The latter fitting procedure is routinely employed in TRANSP modelling of JET experiments, with consistency between measured and computed quantities, such as the neutron rate and plasma stored energy, as a constraint. Both approaches for pulse #94701 provide very similar results. Indeed, for pulse #94704, only the third-order polynomial fitting procedure was employed in the TRANSP simulation, with good agreement (within ~10%) with the measured neutron rate. The equilibrium fitting code EFIT has been used to reconstruct the magnetic equilibrium constrained by magnetics and pressure profiles, that is, including kinetic profiles as well as the contribution of fast ions.

Description of experimental measurements. Mirnov coils are used as a standard MHD diagnostic on almost all tokamak devices. The coils are installed within the vacuum vessel close to the plasma boundary and provide a measurement of the time derivative of the magnetic field. Magnetic spectrograms (Fourier decompositions of the Mirnov coil signal) can then be used to identify relevant oscillation frequencies associated with MHD activity. In JET, a number of coil arrays with high-frequency response are available, allowing activity in the Alfvén range to be observed. The radial localization of the modes was obtained using an X-mode reflectometer (Supplementary information). The ion temperature profiles in this paper were obtained from Charge eXchange Recombination Spectroscopy measurements, and electron temperature profiles from combined analysis of the electron cyclotron emission and high-resolution Thomson scattering diagnostics. The density profiles were taken from high-resolution Thomson scattering measurements, with the density normalized to match the line-averaged density measured by a far-infrared interferometer. The time-resolved neutron yield in JET is measured using three fission chambers, containing ^{235}U and ^{238}U, located outside the vacuum vessel. The time-of-flight spectrometer for rate measures the energy distribution of fusion-born neutrons on the basis of neutron time-of-flight measurements.

Data availability

The JET experimental data are stored in the Processed Pulse File system, which is a centralized data storage and retrieval system for data derived from raw measurements within the JET torus, and from other sources such as simulation programs. These data are fully available for EUROfusion Consortium members and can be accessed by non-members under request to EUROfusion. Numerical data that support the outcome of this study are available from the corresponding authors upon reasonable request.

Code availability

The research codes cited in the paper require prior detailed knowledge of the implemented physics models and are under continuous development. The corresponding authors can be contacted for any further information.

References

44. Brizard, A. J. & Hahm, T. S. Foundations of nonlinear gyrokinetic theory. *Rev. Mod. Phys.* **79**, 421–468 (2007).
45. Merz, F. *Gyrokinetic Simulation of Multimode Plasma Turbulence*. PhD thesis, Univ. Münster (2008).
46. Görler, T. *Multiscale Effects in Plasma Microturbulence*. PhD thesis, Univ. Ulm (2009).
47. Pankin, A., McCune, D., Andre, R., Bateman, G. & Kritz, A. The tokamak Monte Carlo fast ion module NUBEAM in the National Transport Code Collaboration library. *Comp. Phys. Commun.* **159**, 157–184 (2004).
48. Brambilla, M. Numerical simulation of ion cyclotron waves in tokamak plasmas. *Plasma Phys. Control. Fusion* **41**, 1–34 (1999).
49. Grierson, B. A. et al. Orchestrating TRANSP simulations for interpretative and predictive tokamak modeling with OMFIT. *Fusion Sci. Technol.* **74**, 101–115 (2018).

Acknowledgements

We thank M. Baruzzo and F. Nave for the preparation and execution of JET experiments discussed in this paper; E. de la Luna for support in detailing the experimental diagnostics of JET; A. Ho for assistance in processing the experimental data; T. Görler for providing essential advice to ensure the correct numerical setup for the GENE modelling reported in this paper; Y. Camenen, X. Garbet and A. Bierwage for fruitful discussions about the gyrokinetic analyses; G. Giruzzi for valuable suggestions on the article strategy. The simulations were performed on the IRENE Joliot-Curie HPC system, in the framework of the PRACE projects IONFAST and AFIETC, led by J. Garcia, and on the CINECA Marconi HPC within the project GENE4EP, led by D. Zarzoso. This work has been carried out within the framework of the EUROfusion Consortium and has received funding from the Euratom research and training programme 2014-2018 and 2019-2020 under grant agreement no. 633053. The views and opinions express herein do not necessarily reflect those of the European Commission. Part of the work by Ye. O. Kazakov and J.Ongena was also carried out in the framework of projects done for the ITER Scientist Fellow Network (ISFN).

Author contributions

The reported JET experiments were designed and coordinated by Ye. O. Kazakov, M. Nocente, J. Garcia and J. Ongena; S. Mazzi, J. Garcia, D. Zarzoso and S. Benkadda performed gyrokinetic modelling and subsequent analysis, including additional simulations requested by the reviewers. Input data for gyrokinetic modelling were provided by Ž. Štancar, G. Szepesi and M. Dreval. Ž. Štancar performed TRANSP modelling. J. Garcia performed power balance analysis and CRONOS simulations.

M. Dreval provided analysis of the TAE radial location and the correlation reflectometer data. The bispectral analyses were performed by S. Mazzi and D. Zarzoso, J. Eriksson and A. Sahlberg provided neutron measurements data from TOFOR. The original manuscript was written by S. Mazzi, J. Garcia, D. Zarzoso, Ye. O. Kazakov and J. Ongena with feedback from all the authors. Major revisions of this manuscript were undertaken by Ye. O. Kazakov, J. Ongena, J. Garcia and S. Mazzi.

Competing interests

The authors declare no competing interests.

Additional information

Supplementary information The online version contains supplementary material available at https://doi.org/10.1038/s41567-022-01626-8.

Correspondence and requests for materials should be addressed to S. Mazzi or J. Garcia.

Peer review information *Nature Physics* thanks Neal Crocker, Chris Holland and the other, anonymous, reviewer(s) for their contribution to the peer review of this work.

JET Contributors

N. Abid[9], K. Abraham[9], P. Abreu[12], O. Adabonyan[9], P. Adrich[13], M. Afzal[9], T. Ahlgren[14], L. Aho-Mantila[15], N. Aiba[16], M. Airila[15], M. Akhtar[9], R. Albanese[17], M. Alderson-Martin[9], D. Alegre[18], S. Aleiferis[19], A. Aleksa[9], E. Alessi[7], P. Aleynikov[20], J. Algualcil[21], M. Ali[9], M. Allinson[9], B. Alper[9], E. Alves[12], G. Ambrosino[17], R. Ambrosino[17], E. Andersson Sundén[10], P. Andrew[20], B. M. Angelini[22], C. Angioni[23], I. Antoniou[9], L. C. Appel[9], C. Appelbee[9], S. Aria[9], M. Ariola[17], G. Artaserse[22], W. Arter[9], V. Artigues[23], N. Asakura[16], A. Ash[9], N. Ashikawa[24], V. Aslanyan[25], M. Astrain[26], O. Asztalos[27], D. Auld[9], F. Auriemma[28], Y. Austin[9], L. Avotina[29], E. Aymerich[30], A. Baciero[18], F. Bairaktaris[31], J. Balbin[2], L. Balbinot[28], I. Balboa[9], M. Balden[23], C. Balshaw[9], N. Balshaw[9], V. K. Bandaru[23], J. Banks[9], Yu. F. Baranov[9], C. Barcellona[32], A. Barnard[9], M. Barnard[9], R. Barnsley[20], A. Barth[9], M. Baruzzo[22], S. Barwell[9], M. Bassan[20], A. Batista[12], P. Batistoni[22], L. Baumane[29], B. Bauvir[20], L. Baylor[33], P. S. Beaumont[9], D. Beckett[9], A. Begolli[9], M. Beidler[33], N. Bekris[34,35], M. Beldishevski[9], E. Belli[36], F. Belli[22], É. Belonohy[9], M. Ben Yaala[37], J. Benayas[9], J. Bentley[9], H. Bergsåker[38], J. Bernardo[12], M. Bernert[23], M. Berry[9], L. Bertalot[20], H. Betar[39], M. Beurskens[40], S. Bickerton[9], B. Bieg[41], J. Bielecki[42], A. Bierwage[16], T. Biewer[33], R. Bilato[23], P. Bílková[43], G. Birkenmeier[23], H. Bishop[9], J. P. S. Bizarro[12], J. Blackburn[9], P. Blanchard[44], P. Blatchford[9], V. Bobkov[23], A. Boboc[9], P. Bohm[43], T. Bohm[45], I. Bolshakova[46], T. Bolzonella[28], N. Bonanomi[23], D. Bonfiglio[28], X. Bonnin[20], P. Bonofiglo[47], S. Boocock[9], A. Booth[9], J. Booth[9], D. Borba[12,34], D. Borodin[48], I. Borodkina[43,48], C. Boulbe[49], C. Bourdelle[2], M. Bowden[9], K. Boyd[9], I. Božičević Mihalić[50], S. C. Bradnam[9], V. Braic[51], L. Brandt[52], R. Bravanec[53], B. Breizman[54], A. Brett[9], S. Brezinsek[48], M. Brix[9], K. Bromley[9], B. Brown[9], D. Brunetti[7,9], R. Buckingham[9], M. Buckley[9], R. Budny, J. Buermans[3], H. Bufferand[2], P. Buratti[22], A. Burgess[9], A. Buscarino[32], A. Busse[9], D. Butcher[9], E. de la Cal[18], G. Calabrò[55], L. Calacci[56], R. Calado[12], Y. Camenen[1], G. Canal[57], B. Cannas[30], M. Cappelli[22], S. Carcangiu[30], P. Card[9], A. Cardinali[22], P. Carman[9], D. Carnevale[56], M. Carr[9], D. Carralero[18], L. Carraro[28], I. S. Carvalho[12], P. Carvalho[12], I. Casiraghi[6], F. J. Casson[9], C. Castaldo[22], J. P. Catalan[9], N. Catarino[12], F. Causa[7], M. Cavedon[23], M. Cecconello[10], C. D. Challis[9], B. Chamberlain[9], C. S. Chang[47], A. Chankin[23], B. Chapman[9,58], M. Chernyshova[59], A. Chiariello[17], P. Chmielewski[59], A. Chomiczewska[59], L. Chone[60], G. Ciraolo[2], D. Ciric[9], J. Citrin[61], Ł. Ciupinski[62], M. Clark[9], R. Clarkson[9], C. Clements[9], M. Cleverly[9], J. P. Coad[9], P. Coates[9], A. Cobalt[9], V. Coccorese[17], R. Coelho[12], J. W. Coenen[48], I. H. Coffey[63], A. Colangeli[22], L. Colas[2], C. Collins[33], J. Collins[9], S. Collins[9], D. Conka[29], S. Conroy[29], B. Conway[9], N. J. Conway[9], D. Coombs[9], P. Cooper[9], S. Cooper[9], C. Corradino[32], G. Corrigan[9], D. Coster[23], P. Cox[9], T. Craciunescu[64], S. Cramp[9], C. Crapper[9], D. Craven[9], R. Craven[9], M. Crialesi Esposito[52], G. Croci[6], D. Croft[9], A. Croitoru[64], K. Crombé[3,65], T. Cronin[9], N. Cruz[12], C. Crystal[36], G. Cseh[27], A. Cufar[66], A. Cullen[9], M. Curuia[67], T. Czarski[59], H. Dabirikhah[9], A. Dal Molin[6], E. Dale[9], P. Dalgliesh[9], S. Dalley[9], J. Dankowski[42], P. David[23], A. Davies[9], S. Davies[9], G. Davis[9], K. Dawson[9], S. Dawson[9], I. E. Day[9], M. De Bock[20], G. De Temmerman[20], G. De Tommasi[17], K. Deakin[9], J. Deane[9], R. Dejarnac[43], D. Del Sarto[39], E. Delabie[33], D. Del-Castillo-Negrete[33], A. Dempsey[68], R. O. Dendy[9,58], P. Devynck[2], A. Di Siena[23], C. Di Troia[22], T. Dickson[9], P. Dinca[64], T. Dittmar[48], J. Dobrashian[9], R. P. Doerner[69], A. J. H. Donné[70], S. Dorling[9], S. Dormido-Canto[71], D. Douai[2], S. Dowson[9], R. Doyle[68], M. Dreval[4,5], P. Drewelow[40], P. Drews[48], G. Drummond[9], Ph. Duckworth[20], H. Dudding[9,72], R. Dumont[2], P. Dumortier[3], D. Dunai[27], T. Dunatov[50], M. Dunne[23], I. Duran[43], F. Durodié[3], R. Dux[23], A. Dvornova[2], R. Eastham[9], J. Edwards[9], Th. Eich[23], A. Eichorn[9], N. Eidietis[36], A. Eksaeva[48], H. El Haroun[9], G. Ellwood[20], C. Elsmore[9], O. Embreus[73],

S. Emery[9], G. Ericsson[10], B. Eriksson[10], F. Eriksson[74], J. Eriksson[10], L. G. Eriksson[75], S. Ertmer[48], S. Esquembri[26], A. L. Esquisabel[76], T. Estrada[18], G. Evans[9], S. Evans[9], E. Fable[23], D. Fagan[9], M. Faitsch[23], M. Falessi[22], A. Fanni[30], A. Farahani[9], I. Farquhar[9], A. Fasoli[44], B. Faugeras[49], S. Fazinić[50], F. Felici[44], R. Felton[9], A. Fernandes[12], H. Fernandes[12], J. Ferrand[9], D. R. Ferreira[12], J. Ferreira[12], G. Ferrò[56], J. Fessey[9], O. Ficker[43], A. R. Field[9], A. Figueiredo[12,34], J. Figueiredo[12,34], A. Fil[9], N. Fil[9,25], P. Finburg[9], D. Fiorucci[28], U. Fischer[35], G. Fishpool[9], L. Fittill[9], M. Fitzgerald[9], D. Flammini[22], J. Flanagan[9], K. Flinders[9], S. Foley[9], N. Fonnesu[22], M. Fontana[22], J. M. Fontdecaba[18], S. Forbes[9], A. Formisano[17], T. Fornal[59], L. Fortuna[32], E. Fortuna-Zalesna[62], M. Fortune[9], C. Fowler[9], E. Fransson[74], L. Frassinetti[38], M. Freisinger[48], R. Fresa[17], R. Fridström[38], D. Frigione[56], T. Fülöp[73], M. Furseman[9], V. Fusco[22], S. Futatani[77], D. Gadariya[18], K. Gál[70], D. Galassi[44], K. Gałązka[59], S. Galeani[56], D. Gallart[78], R. Galvão[28], Y. Gao[48], J. Garcia[2], M. García-Muñoz[79], M. Gardener[9], L. Garzotti[9], J. Gaspar[80], R. Gatto[81], P. Gaudio[56], D. Gear[9], T. Gebhart[33], S. Gee[9], M. Gelfusa[56], R. George[9], S. N. Gerasimov[9], G. Gervasini[21], M. Gethins[9], Z. Ghani[9], M. Gherendi[64], F. Ghezzi[7], J. C. Giacalone[2], L. Giacomelli[7], G. Giacometti[1], C. Gibson[9], K. J. Gibson[72], L. Gil[12], A. Gillgren[74], E. Giovannozzi[22], C. Giroud[9], R. Glen[9], S. Glöggler[23], J. Goff[9], P. Gohil[36], V. Goloborodko[82], R. Gomes[12], B. Gonçalves[12], M. Goniche[2], A. Goodyear[9], S. Gore[9], G. Gorini[6], T. Görler[23], N. Gotts[9], R. Goulding[47], E. Gow[9], B. Graham[9], J. P. Graves[44], H. Greuner[23], B. Grierson[47], J. Griffiths[9], S. Griph[9], D. Grist[9], W. Gromelski[59], M. Groth[60], R. Grove[33], M. Gruca[59], D. Guard[9], N. Gupta[9], C. Gurl[9], A. Gusarov[83], L. Hackett[9], S. Hacquin[2,34], R. Hager[47], L. Hägg[10], A. Hakola[15], M. Halitovs[29], S. Hall[9], S. A. Hall[9], S. Hallworth-Cook[9], C. J. Ham[9], D. Hamaguchi[16], M. Hamed[2], C. Hamlyn-Harris[9], K. Hammond[9], E. Harford[9], J. R. Harrison[9], D. Harting[9], Y. Hatano[84], D. R. Hatch[54], T. Haupt[9], J. Hawes[9], N. C. Hawkes[9], J. Hawkins[9], T. Hayashi[16], S. Hazael[9], S. Hazel[9], P. Heesterman[9], B. Heidbrink[85], W. Helou[20], O. Hemming[9], S. S. Henderson[9], R. B. Henriques[12], D. Hepple[9], J. Herfindal[33], G. Hermon[9], J. Hill[9], J. C. Hillesheim[9], K. Hizanidis[31], A. Hjalmarsson[10], A. Ho[61], J. Hobirk[23], O. Hoenen[20], C. Hogben[9], A. Hollingsworth[9], S. Hollis[9], E. Hollmann[69], M. Hölzl[23], B. Homan[49], M. Hook[9], D. Hopley[9], J. Horáček[43], D. Horsley[9], N. Horsten[60], A. Horton[9], L. D. Horton[34,44], L. Horvath[9,72], S. Hotchin[9], R. Howell[9], Z. Hu[6], A. Huber[48], V. Huber[48], T. Huddleston[9], G. T. A. Huijsmans[20], P. Huynh[2], A. Hynes[9], D. Imrie[9], M. Imríšek[43], J. Ingleby[9], P. Innocente[28], K. Insulander Björk[73], N. Isernia[17], I. Ivanova-Stanik[59], E. Ivings[9], S. Jablonski[59], S. Jachmich[3,20,34], T. Jackson[9], P. Jacquet[9], H. Järleblad[86], F. Jaulmes[43], J. Jenaro Rodriguez[9], I. Jepu[64], E. Joffrin[2], R. Johnson[9], T. Johnson[38], J. Johnston[9], C. Jones[9], G. Jones[9], L. Jones[9], N. Jones[9], T. Jones[9], A. Joyce[9], R. Juarez[21], M. Juvonen[9], P. Kalnina[29], T. Kaltiaisenaho[15], J. Kaniewski[9], A. Kantor[9], A. Kappatou[23], J. Karhunen[14], D. Karkinsky[9], M. Kaufman[33], G. Kaveney[9], Ye. O. Kazakov[3], V. Kazantzidis[31], D. L. Keeling[9], R. Kelly[9], M. Kempenaars[20], C. Kennedy[9], D. Kennedy[9], J. Kent[9], K. Khan[9], C. Kiefer[23], J. Kilpeläinen[60], C. Kim[36], H.-T. Kim[9,34], S. H. Kim[20], D. B. King[9], R. King[9], D. Kinna[9], V. G. Kiptily[9], A. Kirjasuo[15], K. K. Kirov[9], A. Kirschner[48], T. Kiviniemi[60], G. Kizane[29], M. Klas[87], C. Klepper[33], A. Klix[35], G. Kneale[9], M. Knight[9], P. Knight[9], R. Knights[9], S. Knipe[9], M. Knolker[36], S. Knott[88], M. Kocan[20], F. Köchl[9], I. Kodeli[66], Y. Kolesnichenko[82], Y. Kominis[31], M. Kong[9], V. Korovin[4], B. Kos[66], D. Kos[9], H. R. Koslowski[48], M. Kotschenreuther[54], M. Koubiti[1], E. Kowalska-Strzęciwilk[59], K. Koziol[13], V. Krasilnikov[20], M. Kresina[2,9], K. Krieger[23], N. Krishnan[9], A. Krivska[3], U. Kruezi[20], I. Książek[89], A. B. Kukushkin[16], H. Kumpulainen[60], T. Kurki-Suonio[60], H. Kurotaki[16], S. Kwak[40], O. J. Kwon[90], L. Laguardia[7], E. Lagzdina[29], A. Lahtinen[14], A. Laing[9], N. Lam[9], H. T. Lambertz[48], B. Lane[9], C. Lane[9], E. Lascas Neto[44], E. Łaszyńska[59], K. D. Lawson[9], A. Lazaros[31], E. Lazzaro[7], G. Learoyd[9], C. Lee[91], S. E. Lee[84], S. Leerink[60], T. Leeson[9], X. Lefebvre[9], H. J. Leggate[68], J. Lehmann[9], M. Lehnen[20],

D. Leichtle[35,92], F. Leipold[20], I. Lengar[66], M. Lennholm[9,75], E. Leon Gutierrez[18], B. Lepiavko[82], J. Leppänen[15], E. Lerche[3], A. Lescinskis[29], J. Lewis[9], W. Leysen[83], L. Li[48], Y. Li[48], J. Likonen[15], Ch. Linsmeier[48], B. Lipschultz[72], X. Litaudon[2,34], E. Litherland-Smith[9], F. Liu[2,34], T. Loarer[2], A. Loarte[20], R. Lobel[9], B. Lomanowski[33], P. J. Lomas[9], J. M. López[26], R. Lorenzini[28], S. Loreti[22], U. Losada[18], V. P. Loschiavo[17], M. Loughlin[20], Z. Louka[9], J. Lovell[33], T. Lowe[9], C. Lowry[9,75], S. Lubbad[9], T. Luce[20], R. Lucock[9], C. Luna[93], E. de la Luna[18], M. Lungaroni[56], C. P. Lungu[64], T. Lunt[23], V. Lutsenko[82], B. Lyons[36], A. Lyssoivan[3], M. Machielsen[44], E. Macusova[43], R. Mäenpää[60], C. F. Maggi[9], R. Maggiora[94], M. Magness[9], S. Mahesan[9], H. Maier[3], J. Mailloux[9], R. Maingi[47], K. Malinowski[59], P. Manas[1,23], P. Mantica[7], M. J. Mantsinen[95], J. Manyer[78], A. Manzanares[96], Ph. Maquet[20], G. Marceca[44], C. Marchetto[97], O. Marchuk[48], A. Mariani[7], G. Mariano[22], M. Marin[61], M. Marinelli[56], T. Markovič[43], D. Marocco[22], L. Marot[37], S. Marsden[9], J. Marsh[9], R. Marshall[9], L. Martellucci[56], A. Martin[9], A. J. Martin[9], R. Martone[17], S. Maruyama[20], M. Maslov[9], S. Masuzaki[24], S. Matejcik[35], M. Mattei[17], G. F. Matthews[9], D. Matveev[48], E. Matveeva[43], A. Mauriya[12], F. Maviglia[17], M. Mayer[3], M.-L. Mayoral[9,70], S. Mazzi[1,2], C. Mazzotta[22], R. McAdams[9], P. J. McCarthy[88], K. G. McClements[9], J. McClenaghan[36], P. McCullen[9], D. C. McDonald[9], D. McGuckin[9], D. McHugh[9], G. McIntyre[9], R. McKean[9], J. McKehon[9], B. McMillan[58], L. McNamee[9], A. McShee[9], A. Meakins[9], S. Medley[9], C. J. Meekes[61,98], K. Meghani[9], A. G. Meigs[9], G. Meisl[23], S. Meitner[33], S. Menmuir[9], K. Mergia[19], S. Merriman[9], Ph. Mertens[48], A. Messiaen[3], R. Michling[20], P. Middleton[9], D. Middleton-Gear[9], J. Mietelski[42], D. Milanesio[94], E. Milani[56], F. Militello[9], A. Militello Asp[9], J. Milnes[9], A. Milocco[6], G. Miloshevsky[99], C. Minghao[9], S. Minucci[55], I. Miron[64], M. Miyamoto[100], J. Mlynář[43,101], V. Moiseenko[4], P. Monaghan[9], I. Monakhov[9], T. Moody[9], S. Moon[38], R. Mooney[9], S. Moradi[3], J. Morales[2], R. B. Morales[9], S. Mordijck[102], L. Moreira[9], L. Morgan[9], F. Moro[22], J. Morris[9], K-M. Morrison[9], L. Moser[20,37], D. Moulton[9], T. Mrowetz[9], T. Mundy[9], M. Muraglia[1], A. Murari[28,34], A. Muraro[7], N. Muthusonai[9], B. N'Konga[49], Y.-S. Na[91], F. Nabais[12], M. Naden[9], J. Naish[9], R. Naish[9], F. Napoli[22], E. Nardon[2], V. Naulin[86], M. F. F. Nave[12], I. Nedzelskiy[12], I. Nestoras[9], R. Neu[23], S. Ng[9], M. Nicassio[9], A. H. Nielsen[86], D. Nina[12], D. Nishijima[103], C. Noble[9], C. R. Nobs[9], M. Nocente[6,7], D. Nodwell[9], K. Nordlund[14], H. Nordman[74], R. Normanton[9], J.-M. Noterdaeme[23], S. Nowak[7], E. Nunn[9], H. Nyström[38], M. Oberparleiter[74], B. Obryk[42], J. O'Callaghan[9], T. Odupitan[9], H. J. C. Oliver[9,54], R. Olney[9], M. O'Mullane[104], J. Ongena[3], E. Organ[9], F. Orsitto[17], J. Orszagh[87], T. Osborne[36], R. Otin[9], T. Otsuka[105], A. Owen[9], Y. Oya[106], M. Oyaizu[16], R. Paccagnella[28], N. Pace[9], L. W. Packer[9], S. Paige[9], E. Pajuste[29], D. Palade[64], S. J. P. Pamela[9], N. Panadero[18], E. Panontin[6], A. Papadopoulos[31], G. Papp[23], P. Papp[87], V. V. Parail[9], C. Pardanaud[1], J. Parisi[9,107], F. Parra Diaz[107], A. Parsloe[9], M. Parsons[33], N. Parsons[9], M. Passeri[56], A. Patel[9], A. Pau[44], G. Pautasso[23], R. Pavlichenko[4], A. Pavone[40], E. Pawelec[9], C. Paz Soldan[108], A. Peacock[9,75], M. Pearce[9], E. Peluso[56], C. Penot[20], K. Pepperell[9], R. Pereira[12], T. Pereira[12], E. Perelli Cippo[7], P. Pereslavtsev[35], C. Perez von Thun[59], V. Pericoli[59], D. Perry[9], M. Peterka[43], P. Petersson[38], G. Petravich[27], N. Petrella[9], M. Peyman[9], M. Pillon[22], S. Pinches[20], G. Pintsuk[7], W. Pires de Sá[57], A. Pires dos Reis[57], C. Piron[22], L. Piron[28,109], A. Pironti[17], R. Pitts[20], K. L. van de Plassche[61], N. Platt[9], V. Plyusnin[12], M. Podesta[47], G. Pokol[27], F. M. Poli[47], O. G. Pompilian[64], S. Popovichev[9], M. Poradziński[59], M. T. Porfiri[22], M. Porkolab[25], C. Porosnicu[64], M. Porton[9], G. Poulipoulis[110], I. Predebon[28], G. Prestopino[56], C. Price[9], D. Price[9], M. Price[9], D. Primetzhofer[10], P. Prior[9], G. Provatas[50], G. Pucella[22], P. Puglia[44], K. Purahoo[9], I. Pusztai[73], O. Putignano[9], T. Pütterich[23], A. Quercia[17], E. Rachlew[73], G. Radulescu[33], V. Radulovic[66], M. Rainford[9], P. Raj[35], G. Ralph[9], G. Ramogida[22], D. Rasmussen[33], J. J. Rasmussen[86], G. Rattá[18], S. Ratynskaia[111], M. Rebai[7], D. Réfy[27], R. Reichle[20], M. Reinke[33], D. Reiser[48], C. Reux[2], S. Reynolds[9],

M. L. Richiusa[9], S. Richyal[9], D. Rigamonti[7], F. G. Rimini[9], J. Risner[33], M. Riva[22], J. Rivero-Rodriguez[79], C. M. Roach[9], R. Robins[9], S. Robinson[9], D. Robson[9], P. Rodrigues[12], M. Rodriguez Ramos[50], P. Rodriguez-Fernandez[25], F. Romanelli[22], M. Romanelli[9], S. Romanelli[9], J. Romazanov[48], R. Rossi[56], S. Rowe[9], D. Rowlands[9,34], M. Rubel[38], G. Rubinacci[17], G. Rubino[55], L. Ruchko[57], M. Ruiz[26], J. Ruiz Ruiz[107], C. Ruset[64], J. Rzadkiewicz[13], S. Saarelma[9], E. Safi[14], A. Sahlberg[10], M. Salewski[86], A. Salmi[15], R. Salmon[9], F. Salzedas[12,112], I. Sanders[9], D. Sandiford[9], B. Santos[12], A. Santucci[22], K. Särkimäki[73], R. Sarwar[9], I. Sarychev[9], O. Sauter[44], P. Sauwan[21], N. Scapin[52], F. Schluck[48], K. Schmid[23], S. Schmuck[7], M. Schneider[20], P. A. Schneider[23], D. Schwörer[68], G. Scott[9], M. Scott[9], D. Scraggs[9], S. Scully[9], M. Segato[9], J. Seo[91], G. Sergienko[48], M. Sertoli[9], S. E. Sharapov[9], A. Shaw[9], H. Sheikh[9], U. Sheikh[44], A. Shepherd[9], P. Shigin[20], K. Shinohara[113], S. Shiraiwa[47], D. Shiraki[33], M. Short[9], G. Sias[30], S. A. Silburn[9], A. Silva[12], C. Silva[12], J. Silva[9], D. Silvagni[23], D. Simfukwe[9], J. Simpson[9,60], D. Sinclair[9], S. K. Sipilä[60], A. C. C. Sips[75], P. Sirén[14], A. Sirinelli[20], H. Sjöstrand[10], N. Skinner[9], J. Slater[9], N. Smith[9], P. Smith[9], J. Snell[9], G. Snoep[61], L. Snoj[66], P. Snyder[36], S. Soare[67], E. R. Solano[18], V. Solokha[60], A. Somers[68], C. Sommariva[44], K. Soni[37], E. Sorokovoy[4], M. Sos[43], J. Sousa[12], C. Sozzi[7], S. Spagnolo[28], T. Spelzini[9], F. Spineanu[64], D. Spong[33], D. Sprada[9], S. Sridhar[2], C. Srinivasan[9], G. Stables[9], G. Staebler[36], I. Stamatelatos[19], Ž. Štancar[9,66], P. Staniec[9], G. Stankunas[114], M. Stead[9], E. Stefanikova[38], A. Stephen[9], J. Stephens[9], P. Stevenson[9], M. Stojanov[9], P. Strand[74], H. R. Strauss[115], S. Strikwerda[9], P. Ström[38], C. I. Stuart[9], W. Studholme[9], M. Subramani[9], E. Suchkov[87], S. Sumida[16], H. J. Sun[9], T. E. Susts[29], J. Svensson[40], J. Svoboda[43], R. Sweeney[25], D. Sytnykov[4], T. Szabolics[27], G. Szepesi[9], B. Tabia[9], T. Tadić[50], B. Tál[23], T. Tala[15], A. Tallargio[9], P. Tamain[2], H. Tan[9], K. Tanaka[24], W. Tang[47], M. Tardocchi[7], D. Taylor[9], A. S. Teimane[29], G. Telesca[59], A. Teplukhina[47], D. Terentyev[83], A. Terra[48], D. Terranova[28], N. Terranova[22], D. Testa[44], E. Tholerus[9,38], J. Thomas[9], E. Thoren[111], A. Thorman[9], W. Tierens[23], R. A. Tinguely[25], A. Tipton[9], H. Todd[9], M. Tokitani[24], P. Tolias[111], M. Tomeš[43], A. Tookey[9], Y. Torikai[116], U. von Toussaint[23], P. Tsavalas[19], D. Tskhakaya[43,117], I. Turner[9], M. Turner[9], M. M. Turner[68], M. Turnyanskiy[9,70], G. Tvalashvili[9], S. Tyrrell[9], M. Tyshchenko[82], A. Uccello[7], V. Udintsev[20], G. Urbanczyk[2], A. Vadgama[9], D. Valcarcel[9], M. Valisa[28], P. Vallejos Olivares[38], O. Vallhagen[73], M. Valovič[9], D. Van Eester[3], J. Varje[60], S. Vartanian[2], T. Vasilopoulou[19], G. Vayakis[20], M. Vecsei[27], J. Vega[18], S. Ventre[17], G. Verdoolaege[65], C. Verona[56], G. Verona Rinati[56], E. Veshchev[20], N. Vianello[28], E. Viezzer[79], L. Vignitchouk[111], R. Vila[18], R. Villari[22], F. Villone[17], P. Vincenzi[28], B. Viola[22], A. J. Virtanen[60], A. Vitins[29], Z. Vizvary[9], G. Vlad[22], M. Vlad[64], P. Vondráček[43], P. de Vries[20], B. Wakeling[9], N. R. Walkden[9], M. Walker[9], R. Walker[9], M. Walsh[20], E. Wang[48], N. Wang[9], S. Warder[9], R. Warren[9], J. Waterhouse[9], C. Watts[20], T. Wauters[3], A. Weckmann[38], H. Wedderburn Maxwell[9], M. Weiland[23], H. Weisen[44], M. Weiszflog[10], P. Welch[9], N. Wendler[59], A. West[9], M. Wheatley[9], S. Wheeler[9], A. Whitehead[9], D. Whittaker[9], A. Widdowson[9], S. Wiesen[48], J. Wilkinson[9], J. C. Williams[9], D. Willoughby[9], I. Wilson[9], J. Wilson[9], T. Wilson[9], M. Wischmeier[23], P. Wise[9], G. Withenshaw[9], A. Withycombe[9], D. Witts[9], A. Wojcik-Gargula[42], E. Wolfrum[23], R. Wood[9], C. Woodley[9], R. Woodley[9], B. Woods[9], J. Wright[9], J. C. Wright[25], T. Xu[9], D. Yadikin[74], M. Yajima[24], Y. Yakovenko[82], Y. Yang[20], W. Yanling[48], V. Yanovskiy[43], I. Young[9], R. Young[9], R. J. Zabolockis[29], J. Zacks[9], R. Zagorski[13], F. S. Zaitsev[87], L. Zakharov[14], A. Zarins[29], D. Zarzoso[1], K.-D. Zastrow[9], Y. Zayachuk[9], M. Zerbini[22], W. Zhang[23], Y. Zhou[38], M. Zlobinski[48], A. Zocco[40], A. Zohar[66], V. Zoita[64], S. Zoletnik[27], V. K. Zotta[81], I. Zoulias[9], W. Zwingmann[12] and I. Zychor[13]

[12]Instituto de Plasmas e Fusão Nuclear, Instituto Superior Técnico, Universidade de Lisboa, Lisbon, Portugal. [13]National Centre for Nuclear Research (NCBJ), Otwock-Świerk, Poland. [14]University of Helsinki, Helsinki, Finland. [15]VTT Technical Research Centre of Finland, Espoo, Finland. [16]National Institutes for Quantum and Radiological Science and Technology, Naka, Japan. [17]Consorzio CREATE, Naples, Italy. [18]Laboratorio Nacional de Fusión, CIEMAT, Madrid, Spain. [19]NCSR 'Demokritos' 15310, Agia Paraskevi, Greece. [20]ITER Organization, Saint Paul Lez Durance Cedex, France. [21]Departamento de Ingeniería

Energética, Universidad Nacional de Educación a Distancia, Madrid, Spain. [22]Dipartimento Fusione e Tecnologie per la Sicurezza Nucleare, ENEA C. R. Frascati, Frascati, Italy. [23]Max-Planck-Institut für Plasmaphysik, Garching, Germany. [24]National Institute for Fusion Science, Toki, Japan. [25]MIT Plasma Science and Fusion Center, Cambridge, MA, USA. [26]Grupo I2A2, Universidad Politécnica de Madrid, Madrid, Spain. [27]POB 49, Centre for Energy Research, Budapest, Hungary. [28]Consorzio RFX, Padova, Italy. [29]University of Latvia, Riga, Latvia. [30]Department of Electrical and Electronic Engineering, University of Cagliari, Cagliari, Italy. [31]National Technical University of Athens, Athens, Greece. [32]Dipartimento di Ingegneria Elettrica Elettronica e Informatica, Università degli Studi di Catania, Catania, Italy. [33]Oak Ridge National Laboratory, Oak Ridge, TN, USA. [34]EUROfusion Programme Management Unit, Culham Science Centre, Culham, UK. [35]Karlsruhe Institute of Technology, Karlsruhe, Germany. [36]GENEral Atomics, San Diego, CA, USA. [37]Department of Physics, University of Basel, Basel, Switzerland. [38]Fusion Plasma Physics, EECS, KTH Royal Institute of Technology, Stockholm, Sweden. [39]Institut Jean Lamour, UMR 7198, CNRS-Université de Lorraine, Vandoeuvre-lès-Nancy, France. [40]Teilinstitut Greifswald, Max-Planck-Institut für Plasmaphysik, Greifswald, Germany. [41]Faculty of Marine Engineering, Maritime University of Szczecin, Szczecin, Poland. [42]Institute of Nuclear Physics, Krakov, Poland. [43]Institute of Plasma Physics of the CAS, Prague, Czech Republic. [44]Swiss Plasma Center (SPC), École Polytechnique Fédérale de Lausanne (EPFL), Lausanne, Switzerland. [45]University of Wisconsin-Madison, Madison, WI, USA. [46]Magnetic Sensor Laboratory, Lviv Polytechnic National University, Lviv, Ukraine. [47]Princeton Plasma Physics Laboratory, Princeton, NJ, USA. [48]Forschungszentrum Jülich GmbH, Institut für Energie- und Klimaforschung, TEC Partner, Jülich, Germany. [49]Inria, LJAD, Université Cote d'Azur, CNRS, Nice, France. [50]Ruđer Bošković Institute, Zagreb, Croatia. [51]The National Institute for Optoelectronics, Magurele-Bucharest, Romania. [52]Mechanics, SCI, KTH, Stockholm, Sweden. [53]Fourth State Research, Austin, TX, USA. [54]Institute for Fusion Studies, University of Texas at Austin, Austin, TX, USA. [55]DEIM, University of Tuscia, Viterbo, Italy. [56]Università di Roma Tor Vergata, Rome, Italy. [57]Instituto de Física, Universidade de São Paulo, São Paulo, Brazil. [58]Centre for Fusion, Space and Astrophysics, University of Warwick, Coventry, UK. [59]Institute of Plasma Physics and Laser Microfusion, Warsaw, Poland. [60]Aalto University, Aalto, Finland. [61]FOM Institute DIFFER, Eindhoven, the Netherlands. [62]Warsaw University of Technology, Warsaw, Poland. [63]Astrophysics Research Centre, School of Mathematics and Physics, Queen's University, Belfast, UK. [64]The National Institute for Laser, Plasma and Radiation Physics, Magurele-Bucharest, Romania. [65]Department of Applied Physics, Ghent University, Ghent, Belgium. [66]Jožef Stefan Institute, Slovenian Fusion Association (SFA), Ljubljana, Slovenia. [67]The National Institute for Cryogenics and Isotopic Technology, Râmnicu Vâlcea, Romania. [68]Dublin City University, Dublin, Ireland. [69]University of California at San Diego, La Jolla, CA, USA. [70]EUROfusion Programme Management Unit, Garching, Germany. [71]Departamento de Informática y Automática, Universidad Nacional de Educación a Distancia, Madrid, Spain. [72]York Plasma Institute, Department of Physics, University of York, York, UK. [73]Department of Physics, Chalmers University of Technology, Gothenburg, Sweden. [74]Department of Space, Earth and Environment, Chalmers University of Technology, Gothenburg, Sweden. [75]European Commission, Brussels, Belgium. [76]University of Tennessee, Knoxville, TN, USA. [77]Universitat Politècnica de Catalunya, Barcelona, Spain. [78]Barcelona Supercomputing Center, Barcelona, Spain. [79]Universidad de Sevilla, Seville, Spain. [80]IUSTI, UMR 7343, Aix-Marseille University, CNRS, Marseille, France. [81]Dipartimento di Ingegneria Astronautica, Elettrica ed Energetica, SAPIENZA Università di Roma, Rome, Italy. [82]Institute for Nuclear Research, Kyiv, Ukraine. [83]Studiecentrum voor Kernenergie, Centre d'Etude de l'Energie Nucléaire, Mol, Belgium. [84]University of Toyama, Toyama, Japan. [85]University of California, Irvine, Irvine, CA, USA. [86]Department of Physics, Technical University of Denmark, Kongens Lyngby, Denmark. [87]Department of Experimental Physics, Faculty of Mathematics, Physics and Informatics, Comenius University, Bratislava, Slovakia. [88]University College Cork, Cork, Ireland. [89]Institute of Physics, Opole University, Opole, Poland. [90]Daegu University, Gyeongbuk, Republic of Korea. [91]Department of Nuclear Engineering, Seoul National University, Seoul, Republic of Korea. [92]Fusion for Energy Joint Undertaking, Barcelona, Spain. [93]Arizona State University, Tempe, AZ, USA. [94]Politecnico di Torino, Torino, Italy. [95]ICREA and Barcelona Supercomputing Center, Barcelona, Spain. [96]Universidad Complutense de Madrid, Madrid, Spain. [97]Istituto dei Sistemi Complessi, CNR and Dipartimento di Energia, Politecnico di Torino, Turin, Italy. [98]Eindhoven University of Technology, Eindhoven, the Netherlands. [99]Purdue University, West Lafayette, IN, USA. [100]Department of Material Science, Shimane University, Matsue, Japan. [101]Faculty of Nuclear Sciences and Physical Engineering, Czech Technical University in Prague, Prague, Czech Republic. [102]College of William and Mary, Williamsburg, VA, USA. [103]University of California, Oakland, CA, USA. [104]University of Strathclyde, Glasgow, UK. [105]Kindai University, Osaka, Japan. [106]Shizuoka University, Shizuoka, Japan. [107]Rudolf Peierls Centre for Theoretical Physics, University of Oxford, Oxford, UK. [108]Columbia University, New York, NY, USA. [109]Dipartimento di Fisica "G. Galilei", Università degli Studi di Padova, Padova, Italy. [110]University of Ioannina, Ioannina, Greece. [111]Space and Plasma Physics, EECS, KTH Royal Institute of Technology, Stockholm, Sweden. [112]Faculdade de Engenharia, Universidade do Porto, Porto, Portugal. [113]The University of Tokyo, Kashiwa, Japan. [114]Lithuanian Energy Institute, Kaunas, Lithuania. [115]HRS Fusion, West Orange, NJ, USA. [116]Ibaraki University Graduate School of Science and Engineering, Mito, Japan. [117]Fusion@ÖAW, Österreichische Akademie der Wissenschaften (ÖAW), Technische Universität Wien, Wien, Austria.